Cell Reports

Resource

Single-cell spatial transcriptomic and translatomic profiling of dopaminergic neurons in health, aging, and disease

Graphical abstract

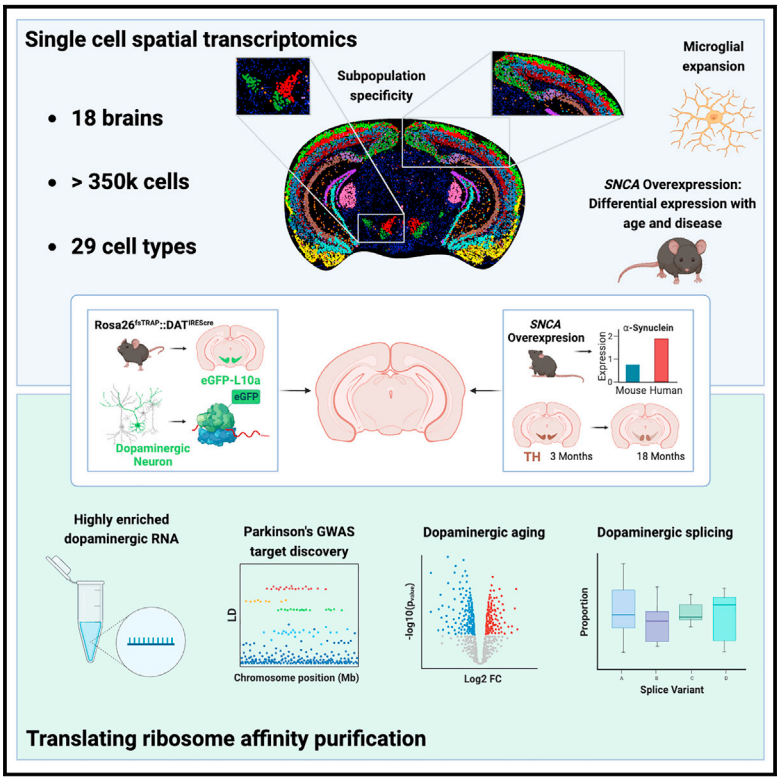

Highlights

- Single-cell spatial transcriptomic study of mouse brain expression in health, age, and disease
- Deep characterization of dopaminergic expression using Stereo-seq and TRAP
- SpatialBrain: resource for expression data exploration

Authors

Peter Kilfeather, Jia Hui Khoo, Katherina Wagner, ..., Natalie Connor-Robson, Zhouchun Shang, Richard Wade-Martins

Correspondence

shangzhouchun@mgi-tech.com (Z.S.), richard.wade-martins@dpag.ox.ac.uk (R.W.-M.)

In brief

Kilfeather et al. showcase a single-cell spatial transcriptomic study of mouse brain spanning 29 cell types. They describe gene expression changes in health, age, and a model of Parkinson's disease. Using TRAP, they further interrogate dopaminergic expression and demonstrate a role for CASR in modulating calcium handling.

Kilfeather et al., 2024, Cell Reports *43*, 113784
March 26, 2024
https://doi.org/10.1016/j.celrep.2024.113784

CellPress

Cell Reports

CellPress
OPEN ACCESS

Resource

Single-cell spatial transcriptomic and translatomic profiling of dopaminergic neurons in health, aging, and disease

Peter Kilfeather,[1,2,3,5] Jia Hui Khoo,[4,5] Katherina Wagner,[1] Han Liang,[4] Maria Claudia Caiazza,[1,2,3] Yanru An,[4] Xingju Zhang,[4] Xiaoyan Chen,[4] Natalie Connor-Robson,[1] Zhouchun Shang,[4,*] and Richard Wade-Martins[1,2,3,6,*]

[1]Oxford Parkinson's Disease Centre and Department of Physiology, Anatomy and Genetics, University of Oxford, Dorothy Crowfoot Hodgkin Building, South Parks Road, Oxford OX1 3QU, UK

[2]Kavli Institute for Nanoscience Discovery, University of Oxford, Dorothy Crowfoot Hodgkin Building, South Parks Road, Oxford OX1 3QU, UK

[3]Aligning Science Across Parkinson's (ASAP) Collaborative Research Network, Chevy Chase, MD, USA

[4]BGI Research, 49276 Riga, Latvia

[5]These authors contributed equally

[6]Lead contact

*Correspondence: shangzhouchun@mgi-tech.com (Z.S.), richard.wade-martins@dpag.ox.ac.uk (R.W.-M.)

https://doi.org/10.1016/j.celrep.2024.113784

SUMMARY

The brain is spatially organized and contains unique cell types, each performing diverse functions and exhibiting differential susceptibility to neurodegeneration. This is exemplified in Parkinson's disease with the preferential loss of dopaminergic neurons of the substantia nigra pars compacta. Using a Parkinson's transgenic model, we conducted a single-cell spatial transcriptomic and dopaminergic neuron translatomic analysis of young and old mouse brains. Through the high resolving capacity of single-cell spatial transcriptomics, we provide a deep characterization of the expression features of dopaminergic neurons and 27 other cell types within their spatial context, identifying markers of healthy and aging cells, spanning Parkinson's relevant pathways. We integrate gene enrichment and genome-wide association study data to prioritize putative causative genes for disease investigation, identifying CASR as a regulator of dopaminergic calcium handling. These datasets represent the largest public resource for the investigation of spatial gene expression in brain cells in health, aging, and disease.

INTRODUCTION

In Parkinson's disease (PD) there is preferential loss of dopaminergic (DA) neurons of the substantia nigra (SN) pars compacta[1,2] and intracellular accumulation of α-synuclein. Characteristic motor signs include tremor, bradykinesia, postural instability, and rigidity, accompanied by non-motor features, including dementia, depression, and psychosis.[3] The disease affects 1% of the global population above the age of 60 years.[4] Age is the biggest risk factor for PD and SN DA neurons may also be lost in healthy aged individuals.[5–7] Overexpression of α-synuclein through locus multiplication causes PD and *in vivo* overexpression of human α-synuclein in the *SNCA*-OVX mouse model recapitulates DA neuron loss.[8,9]

Single-cell RNA sequencing has advanced our understanding of cell-specific expression in complex tissues, such as brain.[10–15] To isolate individual cells, the tissue is dissociated, resulting in destruction of the tissue architecture and gene expression artifacts.[16] Spatial transcriptomics preserves this architecture; however, current sequencing-based spatial technologies do not consistently achieve single-cell or subcellular resolution at high throughput.[17] Fluorescent *in situ* hybridization-based methods offer superior sensitivity at the individual probe level at lower throughput. Spatial enhanced resolution omics sequencing (Stereo-seq) offers nanoscale-resolution spatial expression data, detecting thousands of genes simultaneously.[18]

Single-cell and spatial transcriptomics capture minute quantities of RNA, resulting in lower measurement accuracy compared to bulk RNA sequencing.[19] Translating ribosome affinity purification (TRAP) enables cell-type-specific sequencing with measurement sensitivity comparable to bulk RNA.[20–26] TRAP mRNA is ribosome bound and engaged in translation, providing a more accurate indicator of protein abundance.[27]

TRAP and RiboTag (a related ribosomal profiling technology) have previously been used to study DA neuron gene expression in mice under healthy conditions and after exposure to the toxin, 1-methyl-4-phenyl-1,2,3,6-tetrahydropyridine (MPTP).[26,28,29] The DA neuron aging process has never been characterized using this technology, nor the effects of overexpression of α-synuclein.

Single-cell and single-nuclei RNA sequencing have been used to study DA neuronal expression across a range of species, including humans[11,30,31] and mice.[13,14,32,33] A comparison of aged and young DA neurons, in a spatial context and complemented with data from other brain cell types, is so far lacking.

In this study, we combined the advantages of Stereo-seq and TRAP to characterize the spatial expression signature of individual

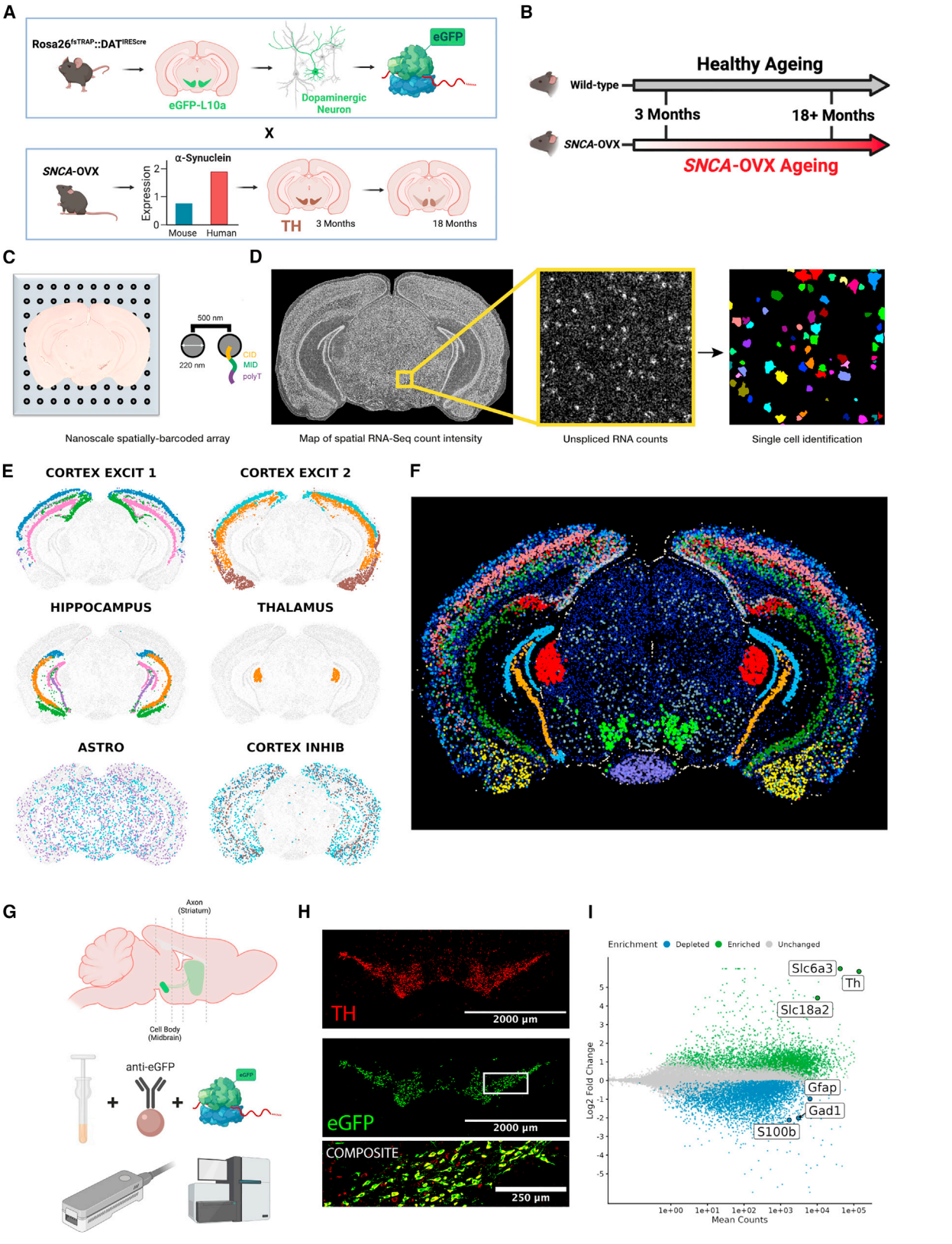

(legend on next page)

cells in mouse brain, with a focus on DA neurons. We optimized a protocol to segment individual cells from Stereo-seq data and subsequently identified 29 cell types across 18 brain sections. By considering the location of each cell, we identified genes with spatially variable expression, such as in SN and ventral tegmental area (VTA) DA neurons. By contrasting DA neuron gene expression with other cell types, we identified strongly specific, yet understudied, markers, including *Slc10a4* and *Cpne7*. Using both long- and short-read sequencing of translating mRNA captured by TRAP, we discovered splice variants specific to DA neurons. We further investigated whether DA axons harbor actively translating ribosomes. To aid the investigation of putative causative genes in PD, we demonstrated how measures of expression specificity from Stereo-seq and TRAP can be used to prioritize candidate genes of interest from GWAS regions. By this process, we identified a role for CASR in regulating intracellular calcium handling in DA neurons. We finally compared aged and young brains, revealing an SN-specific loss of DA neurons and expansion of activated microglia with age. Further, we identified a range of age- and disease-related expression changes in multiple cell types, including DA neurons, spanning multiple PD-relevant pathways.

RESULTS

Integrated transcriptomic profiling in the brain

To combine the advantages of spatial resolution with the sensitivity of the TRAP platform, we generated Rosa26^{fsTRAP}::DAT^{IREScre} (DAT-TRAP) mice, which express eGFP-L10a in DAT-expressing cells (Figure 1A).[34,35] DAT-TRAP mice were crossed with *SNCA*-OVX mice and aged to 18 months to investigate the effects of overexpression of human α-synuclein and aging on DA neuron gene expression (Figures 1A and 1B). TRAP samples were prepared from 56 mice by dissecting the ventral midbrain and the dorsal and ventral striatum, and incubating each homogenate in paramagnetic beads coated in anti-eGFP antibody (STAR Methods; Figure 1G). Stereo-seq samples were prepared from 18 mice by cutting 10-μm cryopreserved sections from fresh frozen brains (STAR Methods).

Stereo-seq single-cell spatial transcriptomic profiling enables the identification and annotation of distinct cell types in the brain

To generate *in situ* transcriptomic data, 18 cryopreserved mouse brain sections were individually mounted onto DNA nanoball-patterned arrays for library preparation. All sections were analyzed as a single group (encompassing both age groups and genotypes) to validate Stereo-seq analysis methodology (Figure 1C; STAR Methods). We produced a spatial map of transcript detection to visualize the intensity of RNA capture across each brain (Figure 1D). In each map, we observed distinct anatomical compartments and cell boundaries. We developed a custom image-processing pipeline to segment individual cells from Stereo-seq brain sections (Figure 1D; STAR Methods; Figure S1 for a detailed example). In the first stage, cells were filtered based on the number of detected genes, to exclude low-complexity cells and putative multiplets (STAR Methods; Figure S2C). Uniform manifold approximation and projection (UMAP) visualization of all 18 brains confirmed that no obvious batch-related differences were present (Figure S2A). We isolated 355,307 high-quality transcriptomes with spatial coordinates from 18 mouse brains. In total, 14,494 genes were detected across all brains, with a median of 626 genes per cell with high-confidence cell segmentation. A summary of the quality control workflow and outcomes is shown in Figure S2C.

Spatial transcriptomics enables the identification and annotation of distinct cell types using both expression and location features. Twenty-nine distinct cell types were consistently identified across all brains sections by unsupervised clustering (STAR Methods; Figures 1E and 1F; summary of all identified cell types in Table S1). Cell types were labeled according to both their anatomical localization and the genes most distinctively expressed (marker genes). For example, neurons were distinguished from glia by the expression of *Snap25* and by patterned localization in regions, such as the hippocampus or thalamus (Figures 1E and 1F). Distinct subpopulations of cells could be visualized, such as neurons of the CA1, CA3, dentate gyrus, and subiculum in the hippocampal region, or GABAergic nuclei within the midbrain. Oligodendrocytes, astrocytes, microglia, and erythrocytes were readily identifiable by marker expression: oligodendrocytes, *Olig1*, *Mbp*, *Sox10*, *Mog*; astrocytes: *Gfap*, *Slc1a3*, *Atp1a2*, *Mt3*; microglia, *Tyrobp/Dap12*, *Ftl1*, *Cts(a/b/d/f/h/l/s/z)*, *Aif1*, *Tmem119*, *Cd68*; erythrocytes, *Hba-* and *Hbb-* genes. Mapping the identity of every cell to its spatial position of origin gives confidence in ascribing greater annotation detail than with expression data alone (e.g., labeling CA1 vs. CA3 hippocampal neurons).

TRAP generates a highly sensitive "translatomic" profile of DA neurons

TRAP complements Stereo-seq by generating a highly sensitive measure of gene expression in a target cell type. In addition,

Figure 1. Integration of Stereo-seq and TRAP for high-resolution gene expression profiling

(A) Transgenic mouse model: Rosa26^{fsTRAP}::DAT^{IREScre} mice were crossed with SNCA-OVX mice to enable the capture of DA mRNA in a model of PD.

(B) Mice were aged to 18+ months in order to study the effect of healthy and Parkinsonian aging.

(C) Stereo-seq array, with spatial transcript map from a single brain section.

(D) Conversion of transcript expression map to segmented individual cells. Segmented cells were subsequently filtered based on transcriptome size and complexity.

(E and F) Demonstration of spatial compartmentalization of annotated cell types: Spatially distinct populations of the cortex, hippocampus, and thalamus can be visualized. Dispersed cell types were also identified (e.g., astrocytes and inhibitory cortical neurons). A total of 29 distinct cell types were identified.

(G) Dissection and TRAP processing schematic, before performing short- and long-read RNA sequencing. eGFP-tagged ribosomes in DAT-expressing cells are captured by anti-GFP antibody-coated paramagnetic beads.

(H) Confirmation of eGFP colocalization with tyrosine hydroxylase (TH), a marker of DA neurons. Scale bars, 2,000 μm for individual channels and 250 μm for the composite.

(I) Demonstration of the specific enrichment of DA marker genes and depletion of marker genes of other neighboring cell types in DAT-TRAP mRNA (n = 56).

mRNA captured by TRAP is engaged in translation, providing a more accurate readout of gene expression compared to conventional transcriptomic technologies.[27] For deep characterization of the DA neuron translatome, short- and long-read sequencing were performed on DAT-TRAP samples (Figure 1G). The dissected ventral midbrain and striatum were processed to enrich for cell body- and putative axon-localized transcripts, respectively. Specific expression of the TRAP transgene was confirmed by immunohistochemical staining for eGFP, which showed distinct colocalization to tyrosine hydroxylase (TH), a marker of DA neurons (Figure 1H). In DAT-TRAP samples, canonical markers of DA neurons were robustly enriched, relative to RNA from bulk tissue homogenate, while markers of other cell types present in the ventral midbrain were depleted (Figures 1I and S2D). We compared our DAT-TRAP enrichment data with those of a public DA neuronal RiboTag dataset[28] and confirmed correlated results, but stronger enrichment of DA genes using TRAP (Figure S2E). Principal-component analysis (PCA) of DAT-TRAP samples showed a major distinction between DAT-TRAP samples and tissue homogenate samples, indicating the importance of using cell-type-specific RNA over bulk homogenate RNA (Figure S2F).

Functionally and spatially distinct populations of DA neurons are detected by single-cell spatial transcriptomic profiling

DA neurons are primarily situated in the ventral midbrain and can be separated into SN and VTA populations by their mediolateral position. SN DA neurons are particularly vulnerable to age-related and Parkinsonian degeneration. By spatially resolving each expression profile, DA neuronal analyses could be focused to those most relevant to PD. We sought to identify DA neurons in our Stereo-seq data and to characterize spatially dependent changes in their expression. In total, 6,378 DA neurons were robustly detected across all 18 brains (Figure 2A). Canonical marker genes, *Th*, *Slc6a3* (DAT), *Ddc* (Dopa decarboxylase), and *Slc18a2* (VMAT2) were strongly enriched in DA neurons, relative to other cell types (Figure 2A). Highly specific markers were also identified with an underreported role in DA function (e.g., *Slc10a4*, *Cpne7*): *SLC10A4* is a member of the bile acid transporter family and regulates vesicular uptake of dopamine.[36] *CPNE7* is a calcium-dependent phospholipid-binding protein that regulates autophagy and axonal/dendritic extension in other cells.[37] To integrate DA neuron-related data from Stereo-seq and TRAP experiments, a meta-analysis was performed across both enrichment comparisons (Figure 2B). Of the top 100 DA neuron markers identified by Stereo-seq, 98 were also enriched in TRAP samples, confirming the strong concordance of both technologies (Figure S3A). The spatial specificity of each marker could be qualitatively confirmed by visualizing the expression of each gene *in situ* (Figure S3C).

We used the coordinate positions of Stereo-seq DA neurons to identify 142 genes with significant evidence of spatially variable expression (false discovery rate [FDR]-adjusted $p < 0.01$; STAR Methods). This revealed a gradient of expression aligning with the SN (e.g., *Cplx1*, *Nrip3*) and VTA (e.g., *Calb1*, *Aldh1a1*) of the ventral midbrain (Figures 2C and 2E). Genes with spatially variable expression in other brain cell types are reported in Table S2. Two-hundred and twenty differentially expressed genes were identified between the two subpopulations (FDR-adjusted $p < 0.05$), including established (VTA, *Calb1*, *Calb2*; SN, *Kcnj6* [*Girk2*], *Cplx1*) and putative markers (SN, *Ndnf*, *Rab3c*, *Rab6b*; VTA, *Ahi1*, *Nnat*). Greater *Sox6* and *Otx2* expression was observed in the SN and VTA, respectively, by determining the number of cells in which each was detected (Figure 2D). The spatial visualization of marker gene expression demonstrated that although an SN-VTA distinction is evident, cells from either population can be found in the other brain region. Where possible, the functional study of DA neurons could benefit from stratification of neurons based on the expression of SN-VTA markers.

TRAP reveals the specificity of transcript expression in DA neurons

To focus on genes actively translated in DA neurons, a measure of gene enrichment was calculated by comparing the abundance of transcripts in DAT-TRAP mRNA and bulk tissue homogenate mRNA. Across all DAT-TRAP samples, 23,292 genes were detected. Of these genes, 4,828 were found to be more abundant compared to TOTAL RNA. This indicated the subset of the transcriptome that is predominantly translated in DA neurons. We next compared DAT-TRAP samples to published TRAP/RiboTag datasets from glutamatergic and GABAergic neurons, astrocytes, microglia, and oligodendrocytes in ventral midbrain. Overall, 2,504 genes were found to be significantly specifically expressed in DA neurons[22,24,38–40] (STAR Methods; FDR-adjusted $p < 0.01$) (Figure S3B). We leveraged the combination of short- and long-read sequencing technology to profile the specific splice variants that define DA neurons: 1,617 alternatively spliced genes were detected, relative to ventral midbrain RNA (Figures S3D and S3E). Interestingly, splicing was not restricted to genes enriched in DAT-TRAP samples: 817 genes demonstrated evidence of differential transcript usage without gene-level enrichment, suggesting that a substantial component of cell-type-specific function could be conferred by splicing and not relative gene-level abundance.

We hypothesized that DA axons locally translate mRNA, due to their extensive projection length into the striatum. We used TRAP to capture putative axonal mRNA from the dorsal and ventral striatum (Figure 1G). In striatal DAT-TRAP samples, we observed an enrichment of 1,803 genes (FDR-adjusted $p < 0.01$), including canonical DA neuron markers, *Th* and *Slc6a3* (DAT) (Figure S4A). We compared our enrichment data with a previously reported proteomic characterization of the striatal DA axonal compartment and found significant overlap between enriched genes/proteins (hypergeometric test, $p = 1.71e{-}29$). The abundance of DA neuron marker genes in striatal DAT-TRAP samples was substantially lower than in midbrain-derived samples, however. We also observed the enrichment of markers of cell types other than DA neurons (e.g., *Gfap*, *Gad1*, *Gad2*). We performed immunohistochemical staining for TH and GFP in mouse brain sections at the level of the striatum (Figure S4B). GFP puncta could be identified that colocalized with TH; however, the overall signal was sparse.

Heritability enrichment analysis identifies CASR as a regulator of intracellular calcium handling in DA neurons

Using Stereo-seq and TRAP data, we designed an approach to prioritize candidate genes for sporadic PD investigation. We

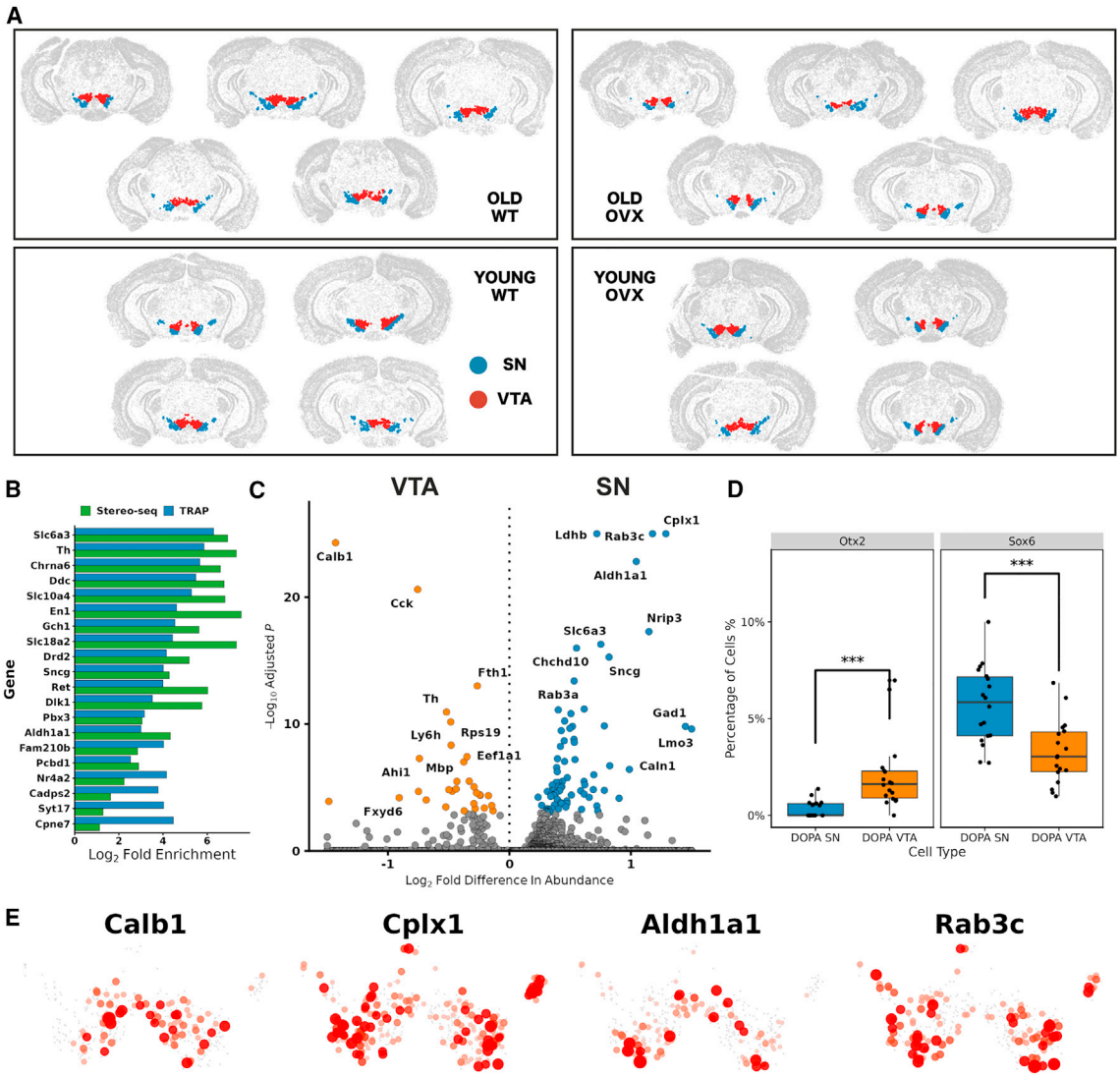

Figure 2. High-resolution single-cell spatial mapping of subpopulations of DA neurons

(A) Confirmation of the spatial distribution of cells annotated as DA neurons.

(B) Top marker genes of DA neurons identified from Stereo-seq and TRAP data, including less commonly recognized *Slc10a4*, *Gap43*, and *Cpne7*. Genes are ranked by the mean fold enrichment in DA neurons from both technologies.

(C) Markers of SN and VTA neuronal populations.

(D) Comparison of *Otx2* and *Sox6* detection rate by region, demonstrating greater expression in VTA and SN, respectively. Whiskers represent the largest value within 1.5× the interquartile range of the first or third quartile. p = 1.99e−5 (*Sox6*) and 4.58e−8 (*Otx2*), logistic regression.

(E) Spatial representation of region-specific marker expression (*Calb1* is VTA; *Cplx1*, *Aldh1a1*, *Rab3c* are SN). n = 18 brains, 6,378 cells for all Stereo-seq analyses, n = 56 for TRAP analyses.

reasoned that enrichment and specificity measures could be used to partition PD heritability according to causative cell types, as demonstrated previously.[33,41] We measured the cell-type-specific enrichment and specificity index (pSI) (STAR Methods) of genes containing SNPs at an $r^2 > 0.5$ and located within ±1 Mb of 107 common risk variants for sporadic PD[42]; 248 out of 303 genes were considered after retaining genes with mouse homologs (Table S3). We observed a broadly neuronal pattern of candidate gene enrichment in Stereo-seq data (Figure 3A), with SN DA neurons demonstrating the greatest mean enrichment. Candidate genes were generally depleted in glial cell types; however, *Ctsb*, *Dpm3*, *Inpp5f*, *Rps12*, *Sbds*, *Scarb2*, and *Stx4a* were commonly enriched between glia and DA neurons (Figure 3A). In TRAP data, DA neurons and oligodendrocytes were jointly found to specifically express the greatest number of candidate genes (Figure 3B). Together, our results indicate a primary role for DA neurons in conferring genetic risk of sporadic PD; however, the common enrichment of a minority of genes across distinct cell types also supports cell-type-agnostic disease processes, as reported previously.[43]

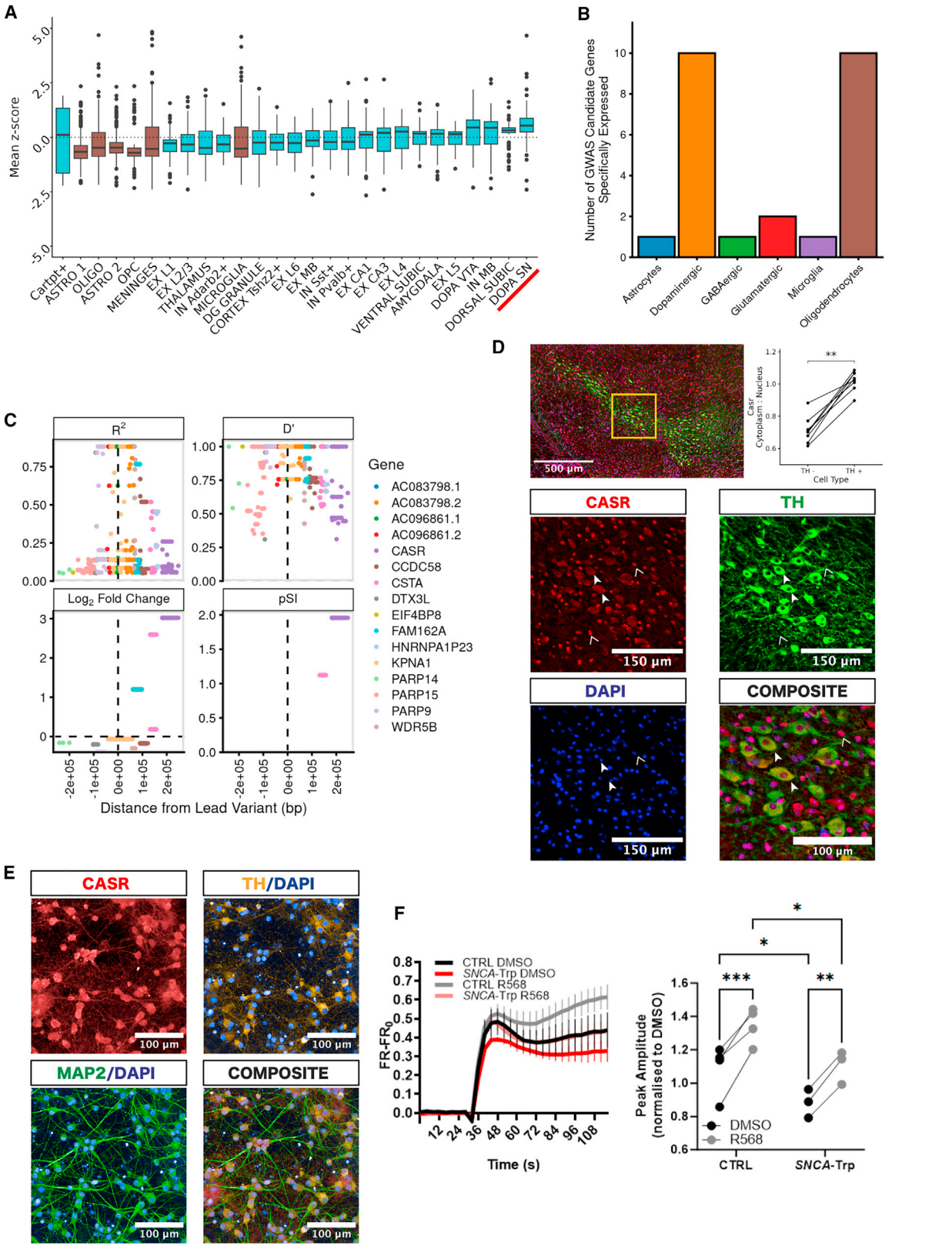

(legend on next page)

We sought to demonstrate how cell-type-specific gene expression could be used to prioritize candidate genes containing variation in linkage disequilibrium with lead PD SNPs. We observed that for 63 out of 91 testable PD GWAS loci, the lead SNP localized to a gene not considered specific or enriched in DAT-TRAP samples. Notable exceptions included rs356182, rs356203, rs256228, rs5019538 (*SNCA*), rs620513 (*FGF20*), rs11158026 (*GCH1*), and rs649339 (*SYT17*), in which the most proximal gene was also the most significantly enriched and specifically expressed. We focused on risk variant rs55961674, an intronic variant of *KPNA1*. In DAT-TRAP samples, *Kpna1* was depleted and in low abundance, relative to bulk ventral midbrain homogenate RNA, indicating low, nonspecific expression in DA neurons. Three candidate genes within the rs55961674 search window were significantly enriched by TRAP, specifically expressed (compared to other TRAP/RiboTag datasets) and contained variants in linkage disequilibrium with the lead SNP (Figure 3C). *Casr*, encoding the calcium sensing receptor, was selected for further investigation, based on demonstrating the most specific expression to DA neurons.

We first validated specific Casr protein expression in DA neurons of the mouse ventral midbrain (Figure 3D). Intriguingly, we observed a distinctly cytoplasmic pattern of expression specifically in DA neurons, while neighboring cells showed depleted cytoplasmic signal and intense nuclear staining. To confirm this difference, we compared the ratio of cytoplasmic to nuclear Casr intensity and found significantly higher cytoplasmic expression in TH-positive than TH-negative cells of the ventral midbrain (Figure 3D; STAR Methods).

We next sought to investigate CASR expression and function in human induced pluripotent stem cell (iPSC)-derived DA neurons. We observed that CASR protein was prominently expressed in TH-positive neurons, with a diffuse cytoplasmic signal (Figure 3E). To evaluate whether CASR protein was functional and able to modulate intracellular calcium levels and dynamics in iPSC-derived DA neurons generated from a patient with PD carrying an *SNCA* triplication mutation, we measured cytoplasmic calcium in cells treated for 1 h with R568 (10 μM), a positive allosteric modulator of CASR.[44] To estimate the levels of calcium stored in the intracellular compartments, we stimulated the cells with ionomycin (5 μM) and measured the increase in cytoplasmatic calcium using Fura-2AM.[45] A significant difference in ionomycin-evoked calcium release was observed between Parkinson's and control iPSC-derived DA neurons before treatment with R568 (Figure 3F). Acute treatment led to increased evoked calcium release in both genotypes, bringing the patient-derived neurons into the range of the healthy control baseline samples (Figure 3F).

By integrating expression specificity data, GWAS summary statistics, and the ability to functionally study gene function in iPSC-derived DA models, we can identify genes with a putative disease role in DA neurons.

Stereo-seq captures age- and disease-induced expression changes across distinct cell types, loss of nigral DA neurons, and neuroinflammatory expansion of microglia

Age remains the most important risk factor for neurodegeneration. We therefore examined aging-related changes in expression across all 29 cell types identified by Stereo-seq (Figure 4A). A range of cell types demonstrated differential expression (FDR-adjusted $p < 0.05$), most notably oligodendrocytes, cortical excitatory neurons of layers 1–3, thalamic neurons, and astrocytes. Pathway enrichment analysis showed that a range of biological processes were affected, including axon ensheathment (oligodendrocytes), regulation of synaptic transmission and intracellular calcium ion homeostasis (excitatory cortical neurons), and regulation of catecholamine secretion (astrocytes).

We next compared gene expression between *SNCA*-OVX and wild-type brains, stratified by age group (Figure 4B). In TRAP samples, overexpression of *SNCA* could be confirmed on a background of normal *Snca* abundance (Figure S4C). No other genes were identified as significantly differentially expressed in DA neurons between control and *SNCA*-OVX by TRAP. In Stereo-seq, changes were detected across a range of cell types (FDR-adjusted $p < 0.05$), especially excitatory and inhibitory midbrain neurons, cortical excitatory neurons of layer 5, and CA1 neurons of the hippocampus. Among the most significantly differentially expressed genes were *Ywhah*, *Ahcyl1*, *Nsamt1*, and *Usp2*, each implicated in PD-relevant areas of biology (Ahycyl1 interacts with Tau, Nsamt1 plays a role in essential tremor, and *Usp2*-deficient mice display altered locomotor activity).

By capturing individual cells, Stereo-seq enabled the comparison of cell number per cell type between conditions. We

Figure 3. Mapping, expression, and function of PD GWAS risk loci

(A) Log_2-fold enrichment or depletion of candidate PD GWAS genes in each annotated cell type from Stereo-seq data. Genes were, with exceptions, generally enriched in neurons and depleted in glia. Whiskers represent the largest value within 1.5× the interquartile range of the first or third quartile.

(B) The number of candidate PD GWAS genes found to be significantly specifically expressed in each TRAP/RiboTag cell type tested. DA neurons and oligodendrocytes jointly specifically expressed the greatest number of candidate genes; n = 56 (DAT-TRAP samples), 6 (GABAergic neurons), 6 (glutamatergic neurons), 3 (oligodendrocytes), 6 (microglia), and 6 (astrocytes).

(C) Linkage disequilibrium measures (R^2 and D′) for rs55961674, indicating the candidacy of >8 genes for consideration. There is significant linkage disequilibrium between the lead SNP and neighboring loci. Log_2-fold change and pSI values indicate enrichment specificity to DA neurons. CASR was the most enriched and specifically expressed candidate gene.

(D) Immunohistochemical confirmation of specific Casr expression in TH-positive cytoplasm of the mouse ventral midbrain (filled arrows). Casr could be detected in neighboring nuclei of TH-negative cells (open arrows). The cytoplasm:nucleus ratio of Casr signal was significantly greater in TH-positive cells; paired Wilcoxon rank-sum text (n = 8, p = 0.0078). Scale bars, 150 μm for individual channels and 100 μm for the composite panel.

(E) Immunocytochemical confirmation of CASR expression in TH-positive iPSC-derived DA neurons. Scale bars, 100 μm for all panels.

(F) Confirmation of CASR-mediated regulation of intracellular Ca^{2+} handling: R568 (a positive allosteric modulator of CASR) increased the Fura2 peak amplitude response to ionomycin administration; n = 3 per genotype; two genotypes; two-way repeated measures analysis of variance (ANOVA) by treatment group and genotype; F = 92.8, p = 0.0006; each colored line in the left panel is a representative trace for each genotype:treatment group.

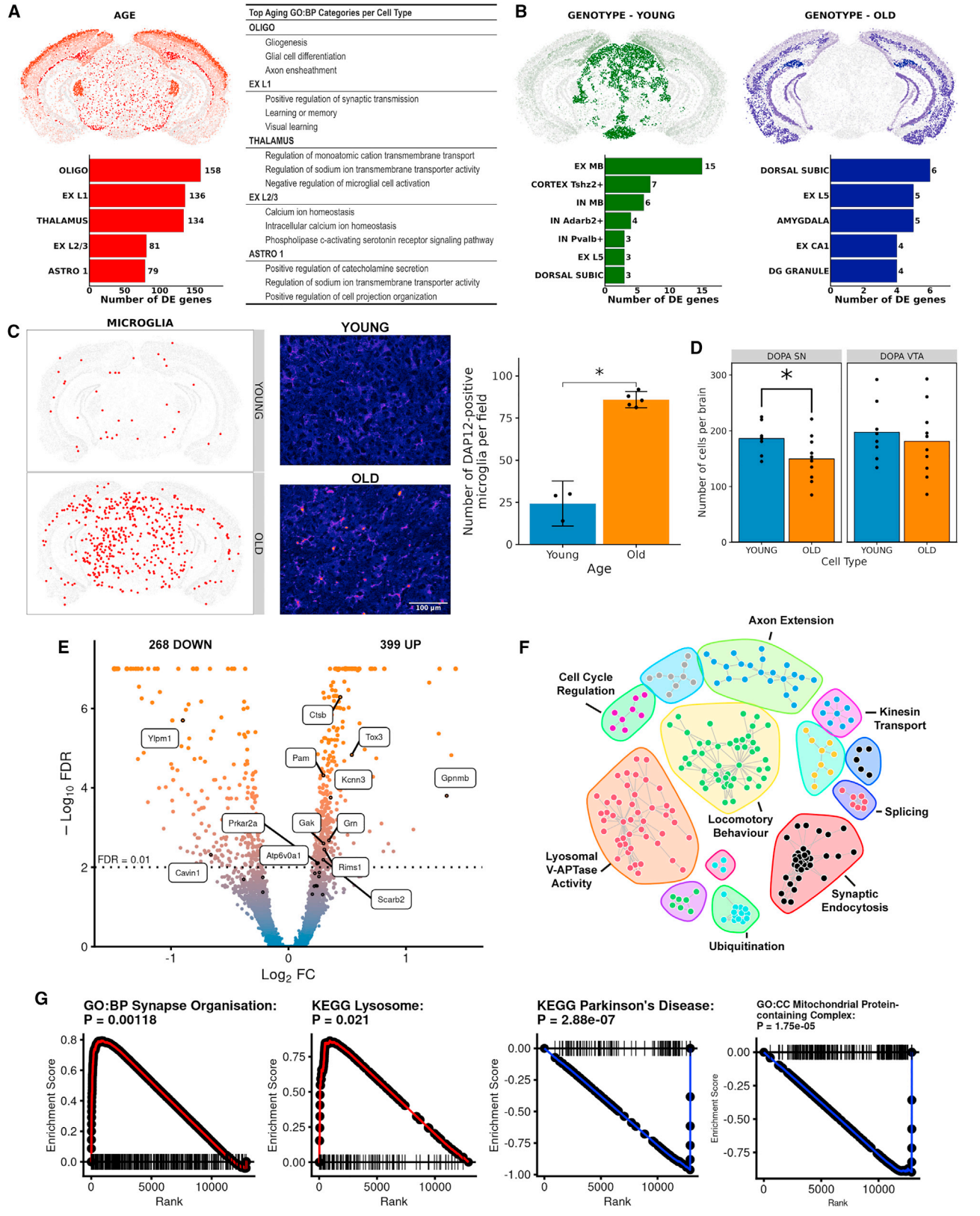

(legend on next page)

detected an expanded microglial population in aged brains (Figure 4C; FDR-adjusted $p < 0.1$). The expansion of activated microglia in aged brains was restricted to the midbrain, corpus callosum, and external capsule. Immunohistochemical staining for Dap12/Tyrobp, a marker of microglia (and the most enriched Stereo-seq marker of this population) confirmed an increase in the number of Dap12-positive cells with a microglial morphology. We also observed an SN-specific loss of DA neurons with age, highlighting the vulnerability of this subpopulation of neurons compared to VTA (Figure 4D).

TRAP reveals the extent of age-induced expression changes in DA neurons

We used TRAP to provide a deeper focus on DA neuron differential gene expression with aging. Greater measurement sensitivity and cohort size led to the discovery of 667 genes with altered expression in aged TRAP samples (399 upregulated, 268 downregulated, FDR-adjusted $p < 0.01$) (Figure 4E). Thirteen candidate PD GWAS genes were among the differentially expressed genes, including *Gpnmb*, also found to be enriched in both DA neurons and oligodendrocytes, and in agreement with previous age-related neuronal findings.[10] We used 1,931 high-confidence protein-protein interactions to subdivide differentially expressed genes into functionally related clusters (Figure 4F; STAR Methods). Each cluster of genes was distinctly enriched for terms related to neuronal function, with particular importance in PD (e.g., lysosomal V-ATPase activity, locomotory behavior, and synaptic endocytosis). By taking the directionality of expression change into account, gene set enrichment analysis further indicated an upregulation of synaptic and lysosomal-related genes (e.g., *Syt1*, *Syt11*, *Sv2a*, *Ap2b1*, *Atp6v0a1*, *Atp6v0d1*, *Atp6v1e1*, and *Atp6ap1*) and a downregulation of mitochondrial and PD-related genes (*mt-Co1*, *mt-Nd1*, *mt-Nd4*, *mt-Nd5*, and *mt-Cyb*) (Figure 4G).

DISCUSSION

In this study, we generated a single-cell-level spatial transcriptomic map of gene expression in the adult mouse brain and produced a high-fidelity translatome-level profile of DA neuron gene expression. By integrating these two data modalities, we characterized the distinctive expression features of DA neurons, demonstrated how expression specificity can be used to prioritize candidate causal genes in PD, and examined the changes that occur in the brain and DA neurons specifically with age.

We identified 29 distinct cell types by unsupervised clustering of cells, based on their expression properties. The spatial compartmentalization of distinct cell types could be mapped to anatomical regions, as in the case of neuronal populations of the hippocampus, thalamus, and midbrain. The ability to spatially visualize each cluster aided the annotation of cell types; however, as methods of spatial transcriptomic analysis develop, we anticipate the integration of spatial information directly into the clustering process, wherein cells with close spatial proximity or patterned localization (e.g., cortical, intestinal and dermal layers) and matched expression are more considered more similar.

The capture area of each Stereo-seq array is 100 mm^2 in this study, larger than existing available spatial transcriptomic technologies (Visium, 42.25 mm^2; Slide-Seq 7.1 mm^2),[46–48] and each Stereo-seq array contains 40 billion capture spots (Visium, 5,000; Slide-Seq, tens of thousands). We leveraged this greater size and density of information to spatially resolve individual cells across the brain. By achieving nanoscale resolution, single-cell spatial data were generated without the need for deconvolution-based methods. We also did not require matched single-cell RNA-seq samples for cell identity annotation.

By integrating Stereo-seq and TRAP data, we identified the expression features most specific to DA neurons in comparison to neighboring cell types. While Stereo-seq provided spatial context, single-cell resolution, and a greater number of unique cell types for comparison, TRAP demonstrated greater measurement sensitivity. By integrating short- and long-read sequencing data from TRAP RNA, we have been able to profile the state of splicing in DA neurons, revealing differential transcript usage across more than a thousand genes. We detected 817 instances of alternative splicing in which individual isoforms were enriched by TRAP, but the overall gene-level count was not. This finding indicates that mouse DA neurons actively translate a larger number of genes than are detectable from only gene-level count data. Our understanding of cell-type-specific expression is strengthened by considering transcript-level expression data.

The single-cell resolution of Stereo-seq enabled the distinction of SN and VTA DA neurons in ventral midbrain. Although we detected subtypes within both populations, we have not reported them here, as their identity could not be accurately predicted

Figure 4. High-resolution age-related changes in gene expression

(A) Spatial representation of cell types ranked by overall aging-associated differential expression. Pathway overrepresentation analysis of each cell type revealed multiple aging-relevant processes.

(B) Spatial representation of cell types ranked by overall genotype-associated differential expression, stratified by age group. The magnitude of differential expression is subtler, compared to age.

(C) Odds ratio analysis of cell type abundance with age in Stereo-seq annotated cell types revealed the expansion of microglia in midbrain, corpus callosum, and the external capsule. Confirmatory immunohistochemical staining for Tyrobp/Dap12, the leading transcriptomic marker of this cell population, confirmed an increase microglial count in aged brain sections. Wilcoxon rank-sum test; n = 3 (young brains), 5 (old brains), $p = 0.036$; data here are represented as the mean ±99% confidence interval. Representative fields from young and old midbrain sections stained for Dap12/Tyrobp (STAR Methods). Scale bar, 100 μm.

(D) A comparison of DA neuron number in SN and VTA confirmed SN-specific loss with age. $p = 0.0213$, mixed model, Poisson regression with mouse of origin as a random effect.

(E) Volcano plot of the fold change and FDR of genes comparing aged and young TRAP samples (n = 56). Thirteen candidate PD GWAS (labeled) genes were within the genes significantly differentially expressed.

(F) Protein-protein interactions among TRAP differentially expressed genes were used to identify functionally distinct clusters.

(G) Gene set enrichment analysis identifies and confirms the up- or downregulation of pathways relevant to aging in DA neurons. Genes related to synaptic organization and lysosomal biology were upregulated with age, as indicated by the enrichment score.

by gene expression in testing data. We expect the addition of further Stereo-seq samples, coupled with improved spatial clustering method development, will lead to the robust identification of further DA neuron subtypes in our data.

We used measures of expression specificity from Stereo-seq and TRAP to demonstrate how genes within disease risk loci can be prioritized for investigation. We showed that candidate causal gene expression was most specific to SN DA neurons, supporting the hypothesis that selective vulnerability may be in part conferred by the selective expression of causative genes.[41] We focused on a window surrounding rs55961674 for study, as this SNP falls within the intronic region of *KPNA1*, a gene considered to not be expressed abundantly or with specificity in DA neurons. By leveraging the sensitivity of TRAP and the diversity of cell types detected in Stereo-seq, we could rank linkage-associated genes surrounding rs55961674 by their expression specificity. We demonstrated specific DA cytoplasmic expression of CASR in two model systems (mouse and human) and showed that CASR regulates intracellular calcium handling in human DA neurons. The specificity of cytoplasmic CASR expression to DA neurons and demonstration of its functional role in regulating intracellular calcium handling indicates that variation in this gene could contribute to PD disease risk. Long-term functional study of this gene is of interest, such as by generating a DA neuron-selective knockout *Casr* mouse model.

The large capture area of the Stereo-seq array, combined with single-cell-level resolution, enabled parallel region-dependent and cell-type-dependent comparison. We identified an age-dependent reduction in SN DA neuron cell number. This supports previous findings that DA neuron number declines with age[1,2] and demonstrates the ability of Stereo-seq to identify a subtype of DA neuron that is most vulnerable to aging. In addition, we detected and confirmed the expansion of microglia with age, expressing a variety of pro-inflammatory markers. Previous investigations into changes in microglial number with age have reported disparate findings, depending on the species and brain region investigated.[10,49,50] However, age-related neuroinflammation has been shown previously to significantly contribute to degeneration in PD.[51]

A surprising finding in this study was the absence of detectable gene expression changes in DA neurons due to *SNCA* overexpression. The age-dependent pattern of SN DA neuronal loss in *SNCA*-OVX mice is considered to recapitulate the slow progression of PD pathology in patients. We would suggest that the transcriptional effects of *SNCA* overexpression (at the level achieved by the *SNCA*-OVX model) are subtle. To capture DA neuron-specific gene expression changes induced by the interaction of *SNCA* overexpression and aging, it may be necessary to sample a greater number of time points and replicates. In addition, the *SNCA*-OVX mice used in this study also expressed *Snca* (STAR Methods). The expression of wild-type *Snca* may ameliorate disease-related pathology previously observed in $Snca^{-/-}$ *SNCA*-OVX mice. However, our Stereo-seq analysis did enable the detection of transcriptional changes due to *SNCA* overexpression in other cell types.

We leveraged the sensitivity of TRAP to assess the evidence for axonal translation in DA neurons. We observed enrichment of DA markers, *Th*, *Slc6a3* (*DAT*), and *Slc18a2* (*VMAT2*) in striatal TRAP samples; however, we also observed enrichment of markers of other cell types. Furthermore, the abundance of DA markers in striatal TRAP samples was markedly lower than in midbrain-derived samples. We detected GFP puncta in striatum that colocalized with TH, although overall signal was sparse.

Hobson et al. previously used RiboTag, a similar technology to TRAP, to study axonal translation in DA neurons and concluded that there was no evidence for the process occurring. We conclude that we do see evidence for axonal translation in DA neurons by TRAP, although we suggest that the scale of activity is substantially lower than at the level of the cell body. The enrichment of markers of other cell types in striatal TRAP samples also indicates the likelihood of low-level ectopic expression of the eGFP-L10a transgene in neighboring cells, as has been reported in DAT-Cre lines.[52]

Limitations of the study

An ongoing challenge for droplet-based single-cell and emerging spatial transcriptomic technologies will be to increase the sensitivity of gene detection. Lower detection sensitivity leads to zero inflation, in which many genes are detected at the population level but are largely undetectable at the individual cell level.[53,54] The power to detected differential expression is limited by zero inflation. Lateral diffusion of RNA also limits the resolving capacity of current spatial transcriptomic methods.[55] To minimize the impact of diffusion, we segmented individual cells by spatial read intensity, excluding lower-intensity background regions. In addition, we excluded all cells that co-expressed markers of neurons and glia. TRAP demonstrated greater detection power (over 15,000 genes per sample), offering the most inclusive and sensitive measure of DA gene expression currently available. The limitation of TRAP is its specificity to cell subpopulations. DA neurons of the SN and VTA could not be reliably separated during tissue processing due to their proximity, so measurements reflect the averaged expression of these regions. With greater detection sensitivity and/or sample number, further DA neuron subpopulations may become identifiable.

Together, our spatial transcriptomic and translatome profiling of DA neurons represent a valuable resource to the neuroscience community. Our spatial data can be used to prioritize candidate causal genes involved in conferring genetic risk of brain-related diseases other than PD. In addition, these data can be used as a reference for the development of analytical approaches to spatial research. Our TRAP data provide a reference for the querying of genes or isoforms specific to DA neurons in health and with age. We have combined all results from analyses in this study into a database for public access: spatialbrain.org.

STAR★METHODS

Detailed methods are provided in the online version of this paper and include the following:

- KEY RESOURCES TABLE
- RESOURCE AVAILABILITY
  - Lead contact
  - Materials availability
  - Data and code availability

SUPPLEMENTAL INFORMATION

Supplemental information can be found online at https://doi.org/10.1016/j.celrep.2024.113784.

ACKNOWLEDGMENTS

This research was funded in part by Aligning Science Across Parkinson's (ASAP-020370) through the Michael J. Fox Foundation for Parkinson's Research (MJFF), in part by the Monument Trust Discovery Award from Parkinson's UK (J-1403), and in part by Science, Technology and Innovation Commission of Shenzhen Municipality under grant no. JCYJ20180507183628543. We sincerely thank the support provided by China National GeneBank. For the purpose of open access, the author has applied a CC BY 4.0 public copyright license to all author accepted manuscripts arising from this submission. P.K. was supported by a Medical Research Council studentship and post-doctoral fellowship; K.W. was supported by a Parkinson's UK studentship (H-1301); and M.C.C. is supported by the Wellcome Trust (grant ref. 223202/Z/21/Z) and previously held the Joan Pitts-Tucker/Heyman Moritz Studentship.

AUTHOR CONTRIBUTIONS

P.K. performed all analyses, with help from J.H.K. and H.L. P.K. and K.W. optimized and performed TRAP experiments. P.K. performed all long-read sequencing experiments, all immunohistochemistry experiments, and all tissue collection for Stereo-seq. M.C.C. performed all Fura-2 CASR and iPSC ICC experiments. Y.A., J.H.K., X.Z., and X.C. performed the Stereo-seq experiments. N.C.-R. co-supervised the project and contributed to project and experimental design. R.W.M. conceived the project. R.W.M. and Z.S. supervised the entire study and secured funding. P.K. and R.W.M. wrote the paper, with contributions from all authors. All authors reviewed the manuscript and approved its submission.

DECLARATION OF INTERESTS

The authors declare no competing interests.

Received: April 12, 2023
Revised: November 14, 2023
Accepted: January 27, 2024
Published: February 21, 2024

REFERENCES

1. Dickson, D.W., Braak, H., Duda, J.E., Duyckaerts, C., Gasser, T., Halliday, G.M., Hardy, J., Leverenz, J.B., Del Tredici, K., Wszolek, Z.K., and Litvan, I. (2009). Neuropathological assessment of Parkinson's disease: refining the diagnostic criteria. Lancet Neurol. *8*, 1150–1157.
2. Halliday, G.M., Holton, J.L., Revesz, T., and Dickson, D.W. (2011). Neuropathology underlying clinical variability in patients with synucleinopathies. Acta Neuropathol. *122*, 187–204.
3. Gelb, D.J., Oliver, E., and Gilman, S. (1999). Diagnostic Criteria for Parkinson Disease. Arch. Neurol. *56*, 33–39.
4. Baker, M.G., and Graham, L. (2004). The journey: Parkinson's disease. BMJ *329*, 611–614.
5. de Lau, L.M.L., and Breteler, M.M.B. (2006). Epidemiology of Parkinson's disease. Lancet Neurol. *5*, 525–535.
6. Fearnley, J.M., and Lees, A.J. (1991). Ageing and Parkinson's disease: substantia nigra regional selectivity. Brain *114*, 2283–2301.
7. McGeer, P.L., McGeer, E.G., and Suzuki, J.S. (1977). Aging and Extrapyramidal Function. Arch. Neurol. *34*, 33–35.
8. Janezic, S., Threlfell, S., Dodson, P.D., Dowie, M.J., Taylor, T.N., Potgieter, D., Parkkinen, L., Senior, S.L., Anwar, S., Ryan, B., et al. (2013). Deficits in dopaminergic transmission precede neuron loss and dysfunction in a new Parkinson model. Proc. Natl. Acad. Sci. USA *110*, E4016–E4025.
9. Hunn, B.H.M., Vingill, S., Threlfell, S., Alegre-Abarrategui, J., Magdelyns, M., Deltheil, T., Bengoa-Vergniory, N., Oliver, P.L., Cioroch, M., Doig, N.M., et al. (2019). Impairment of Macroautophagy in Dopamine Neurons Has Opposing Effects on Parkinsonian Pathology and Behavior. Cell Rep. *29*, 920–931.e7.
10. Ximerakis, M., Lipnick, S.L., Innes, B.T., Simmons, S.K., Adiconis, X., Dionne, D., Mayweather, B.A., Nguyen, L., Niziolek, Z., Ozek, C., et al. (2019). Single-cell transcriptomic profiling of the aging mouse brain. Nat. Neurosci. *22*, 1696–1708.
11. Kamath, T., Abdulraouf, A., Burris, S.J., Langlieb, J., Gazestani, V., Nadaf, N.M., Balderrama, K., Vanderburg, C., and Macosko, E.Z. (2022). Single-cell genomic profiling of human dopamine neurons identifies a population that selectively degenerates in Parkinson's disease. Nat. Neurosci. *25*, 588–595.
12. Zeisel, A., Muñoz-Manchado, A.B., Codeluppi, S., Lönnerberg, P., La Manno, G., Juréus, A., Marques, S., Munguba, H., He, L., Betsholtz, C., et al. (2015). Cell types in the mouse cortex and hippocampus revealed by single-cell RNA-seq. Science *347*, 1138–1142.
13. La Manno, G., Gyllborg, D., Codeluppi, S., Nishimura, K., Salto, C., Zeisel, A., Borm, L.E., Stott, S.R.W., Toledo, E.M., Villaescusa, J.C., et al. (2016). Molecular Diversity of Midbrain Development in Mouse, Human, and Stem Cells. Cell *167*, 566–580.e19.
14. Poulin, J.-F., Gaertner, Z., Moreno-Ramos, O.A., and Awatramani, R. (2020). Classification of Midbrain Dopamine Neurons Using Single-Cell Gene Expression Profiling Approaches. Trends Neurosci. *43*, 155–169.
15. Poulin, J.-F., Zou, J., Drouin-Ouellet, J., Kim, K.Y.A., Cicchetti, F., and Awatramani, R.B. (2014). Defining Midbrain Dopaminergic Neuron Diversity by Single-Cell Gene Expression Profiling. Cell Rep. *9*, 930–943.
16. van den Brink, S.C., Sage, F., Vértesy, Á., Spanjaard, B., Peterson-Maduro, J., Baron, C.S., Robin, C., and van Oudenaarden, A. (2017). Single-cell sequencing reveals dissociation-induced gene expression in tissue subpopulations. Nat. Methods *14*, 935–936.
17. Moses, L., and Pachter, L. (2022). Museum of spatial transcriptomics. Nat. Methods *19*, 534–546.
18. Chen, A., Liao, S., Cheng, M., Ma, K., Wu, L., Lai, Y., Qiu, X., Yang, J., Xu, J., Hao, S., et al. (2022). Spatiotemporal transcriptomic atlas of mouse organogenesis using DNA nanoball-patterned arrays. Cell *185*, 1777–1792.e21.

19. Svensson, V., Natarajan, K.N., Ly, L.H., Miragaia, R.J., Labalette, C., Macaulay, I.C., Cvejic, A., and Teichmann, S.A. (2017). Power Analysis of Single Cell RNA-Sequencing Experiments. Nat. Methods *14*, 381–387.

20. Heiman, M., Kulicke, R., Fenster, R.J., Greengard, P., and Heintz, N. (2014). Cell type–specific mRNA purification by translating ribosome affinity purification (TRAP). Nat. Protoc. *9*, 1282–1291.

21. Dougherty, J.D., Fomchenko, E.I., Akuffo, A.A., Schmidt, E., Helmy, K.Y., Bazzoli, E., Brennan, C.W., Holland, E.C., and Milosevic, A. (2012). Candidate pathways for promoting differentiation or quiescence of oligodendrocyte progenitor-like cells in glioma. Cancer Res. *72*, 4856–4868.

22. Dougherty, J.D., Maloney, S.E., Wozniak, D.F., Rieger, M.A., Sonnenblick, L., Coppola, G., Mahieu, N.G., Zhang, J., Cai, J., Patti, G.J., et al. (2013). The disruption of Celf6, a gene identified by translational profiling of serotonergic neurons, results in autism-related behaviors. J. Neurosci. *33*, 2732–2753.

23. Doyle, J.P., Dougherty, J.D., Heiman, M., Schmidt, E.F., Stevens, T.R., Ma, G., Bupp, S., Shrestha, P., Shah, R.D., Doughty, M.L., et al. (2008). Application of a translational profiling approach for the comparative analysis of CNS cell types. Cell *135*, 749–762.

24. Sakers, K., Lake, A.M., Khazanchi, R., Ouwenga, R., Vasek, M.J., Dani, A., and Dougherty, J.D. (2017). Astrocytes locally translate transcripts in their peripheral processes. Proc. Natl. Acad. Sci. USA *114*, E3830–E3838.

25. Shigeoka, T., Jung, H., Jung, J., Turner-Bridger, B., Ohk, J., Lin, J.Q., Amieux, P.S., and Holt, C.E. (2016). Dynamic Axonal Translation in Developing and Mature Visual Circuits. Cell *166*, 181–192.

26. Hobson, B.D., Kong, L., Angelo, M.F., Lieberman, O.J., Mosharov, E.V., Herzog, E., Sulzer, D., and Sims, P.A. (2022). Subcellular and regional localization of mRNA translation in midbrain dopamine neurons. Cell Rep. *38*, 110208.

27. Blevins, W.R., Tavella, T., Moro, S.G., Blasco-Moreno, B., Closa-Mosquera, A., Díez, J., Carey, L.B., and Albà, M.M. (2019). Extensive post-transcriptional buffering of gene expression in the response to severe oxidative stress in baker's yeast. Sci. Rep. *9*, 11005.

28. Brichta, L., Shin, W., Jackson-Lewis, V., Blesa, J., Yap, E.L., Walker, Z., Zhang, J., Roussarie, J.P., Alvarez, M.J., Califano, A., et al. (2015). Identification of neurodegenerative factors using translatome-regulatory network analysis. Nat. Neurosci. *18*, 1325–1333.

29. Dougherty, J.D. (2017). Generation and characterization of a mouse line for monitoring translation in dopaminergic neurons. Sci. Rep. *7*, 8117.

30. Smajić, S., Prada-Medina, C.A., Landoulsi, Z., Ghelfi, J., Delcambre, S., Dietrich, C., Jarazo, J., Henck, J., Balachandran, S., Pachchek, S., et al. (2022). Single-cell sequencing of human midbrain reveals glial activation and a Parkinson-specific neuronal state. Brain *145*, 964–978.

31. Agarwal, D., Sandor, C., Volpato, V., Caffrey, T.M., Monzón-Sandoval, J., Bowden, R., Alegre-Abarrategui, J., Wade-Martins, R., and Webber, C. (2020). A single-cell atlas of the human substantia nigra reveals cell-specific pathways associated with neurological disorders. Nat. Commun. *11*, 4183.

32. Saunders, A., Macosko, E.Z., Wysoker, A., Goldman, M., Krienen, F.M., de Rivera, H., Bien, E., Baum, M., Bortolin, L., Wang, S., et al. (2018). Molecular Diversity and Specializations among the Cells of the Adult Mouse Brain. Cell *174*, 1015–1030.e16.

33. Hook, P.W., McClymont, S.A., Cannon, G.H., Law, W.D., Morton, A.J., Goff, L.A., and McCallion, A.S. (2018). Single-Cell RNA-Seq of Mouse Dopaminergic Neurons Informs Candidate Gene Selection for Sporadic Parkinson Disease. Am. J. Hum. Genet. *102*, 427–446.

34. Zhou, P., Zhang, Y., Ma, Q., Gu, F., Day, D.S., He, A., Zhou, B., Li, J., Stevens, S.M., Romo, D., and Pu, W.T. (2013). Interrogating translational efficiency and lineage-specific transcriptomes using ribosome affinity purification. Proc. Natl. Acad. Sci. USA *110*, 15395–15400.

35. Bäckman, C.M., Malik, N., Zhang, Y., Shan, L., Grinberg, A., Hoffer, B.J., Westphal, H., and Tomac, A.C. (2006). Characterization of a mouse strain expressing Cre recombinase from the 3' untranslated region of the dopamine transporter locus. Genesis *44*, 383–390.

36. Larhammar, M., Patra, K., Blunder, M., Emilsson, L., Peuckert, C., Arvidsson, E., Rönnlund, D., Preobraschenski, J., Birgner, C., Limbach, C., et al. (2015). SLC10A4 Is a Vesicular Amine-Associated Transporter Modulating Dopamine Homeostasis. Biol. Psychiatry *77*, 526–536.

37. Park, Y.-H., Son, C., Seo, Y.M., Lee, Y.S., Har, A., and Park, J.C. (2021). CPNE7-Induced Autophagy Restores the Physiological Function of Mature Odontoblasts. Front. Cell Dev. Biol. *9*, 655498.

38. Paul, E.J., Tossell, K., and Ungless, M.A. (2019). Transcriptional profiling aligned with in situ expression image analysis reveals mosaically expressed molecular markers for GABA neuron sub-groups in the ventral tegmental area. Eur. J. Neurosci. *50*, 3732–3749.

39. Voskuhl, R.R., Itoh, N., Tassoni, A., Matsukawa, M.A., Ren, E., Tse, V., Jang, E., Suen, T.T., and Itoh, Y. (2019). Gene expression in oligodendrocytes during remyelination reveals cholesterol homeostasis as a therapeutic target in multiple sclerosis. Proc. Natl. Acad. Sci. USA *116*, 10130–10139.

40. Ouwenga, R., Lake, A.M., Aryal, S., Lagunas, T., and Dougherty, J.D. (2018). The Differences in Local Translatome across Distinct Neuron Types Is Mediated by Both Baseline Cellular Differences and Post-transcriptional Mechanisms. eNeuro *5*. ENEURO.0320-418.2018.2018.

41. Finucane, H.K., Reshef, Y.A., Anttila, V., Slowikowski, K., Gusev, A., Byrnes, A., Gazal, S., Loh, P.R., Lareau, C., Shoresh, N., et al. (2018). Heritability enrichment of specifically expressed genes identifies disease-relevant tissues and cell types. Nat. Genet. *50*, 621–629.

42. Nalls, M.A., Blauwendraat, C., Vallerga, C.L., Heilbron, K., Bandres-Ciga, S., Chang, D., Tan, M., Kia, D.A., Noyce, A.J., Xue, A., et al. (2019). Identification of novel risk loci, causal insights, and heritable risk for Parkinson's disease: a meta-analysis of genome-wide association studies. Lancet Neurol. *18*, 1091–1102.

43. Reynolds, R.H., Botía, J., Nalls, M.A., International Parkinson's Disease Genomics Consortium IPDGC; System Genomics of Parkinson's Disease SGPD; Hardy, J., Gagliano Taliun, S.A., and Ryten, M. (2019). Moving beyond neurons: the role of cell type-specific gene regulation in Parkinson's disease heritability. NPJ Park. Dis. *5*, 6–14.

44. Fox, J., Lowe, S.H., Petty, B.A., and Nemeth, E.F. (1999). NPS R-568: a type II calcimimetic compound that acts on parathyroid cell calcium receptor of rats to reduce plasma levels of parathyroid hormone and calcium. J. Pharmacol. Exp. Ther. *290*, 473–479.

45. Grynkiewicz, G., Poenie, M., and Tsien, R.Y. (1985). A new generation of Ca2+ indicators with greatly improved fluorescence properties. J. Biol. Chem. *260*, 3440–3450.

46. What is the spatial resolution and configuration of the capture area of the Visium Gene Expression Slide?. 10X Genomics https://kb.10xgenomics.com/hc/en-us/articles/360035487572-What-is-the-spatial-resolution-and-configuration-of-the-capture-area-of-the-Visium-Gene-Expression-Slide-.

47. Rodriques, S.G., Stickels, R.R., Goeva, A., Martin, C.A., Murray, E., Vanderburg, C.R., Welch, J., Chen, L.M., Chen, F., and Macosko, E.Z. (2019). Slide-seq: A scalable technology for measuring genome-wide expression at high spatial resolution. Science *363*, 1463–1467.

48. Stickels, R.R., Murray, E., Kumar, P., Li, J., Marshall, J.L., Di Bella, D.J., Arlotta, P., Macosko, E.Z., and Chen, F. (2021). Highly sensitive spatial transcriptomics at near-cellular resolution with Slide-seqV2. Nat. Biotechnol. *39*, 313–319.

49. Grabert, K., Michoel, T., Karavolos, M.H., Clohisey, S., Baillie, J.K., Stevens, M.P., Freeman, T.C., Summers, K.M., and McColl, B.W. (2016). Microglial brain region−dependent diversity and selective regional sensitivities to aging. Nat. Neurosci. *19*, 504–516.

50. Salas, I.H., Burgado, J., and Allen, N.J. (2020). victims or villains of the aging brain? Neurobiol. Dis. *143*, 105008.

51. Tansey, M.G., Wallings, R.L., Houser, M.C., Herrick, M.K., Keating, C.E., and Joers, V. (2022). Inflammation and immune dysfunction in Parkinson disease. Nat. Rev. Immunol. *22*, 657–673.

52. Papathanou, M., Dumas, S., Pettersson, H., Olson, L., and Wallén-Mackenzie, Å. (2019). Off-Target Effects in Transgenic Mice: Characterization of Dopamine Transporter (DAT)-Cre Transgenic Mouse Lines Exposes Multiple Non-Dopaminergic Neuronal Clusters Available for Selective Targeting within Limbic Neurocircuitry. eNeuro *6*. ENEURO.0198-19.

53. Risso, D., Perraudeau, F., Gribkova, S., Dudoit, S., and Vert, J.-P. (2018). A general and flexible method for signal extraction from single-cell RNA-seq data. Nat. Commun. *9*, 284.

54. Van den Berge, K., Perraudeau, F., Soneson, C., Love, M.I., Risso, D., Vert, J.P., Robinson, M.D., Dudoit, S., and Clement, L. (2018). Observation weights unlock bulk RNA-seq tools for zero inflation and single-cell applications. Genome Biol. *19*, 24.

55. Larsson, L., Frisén, J., and Lundeberg, J. (2021). Spatially resolved transcriptomics adds a new dimension to genomics. Nat. Methods *18*, 15–18.

56. Vasek, M.J., Mueller, S.M., Fass, S.B., Deajon-Jackson, J.D., Liu, Y., Crosby, H.W., Koester, S.K., Yi, J., Li, Q., and Dougherty, J.D. (2023). Local translation in microglial processes is required for efficient phagocytosis. Nat. Neurosci. *26*, 1185–1195.

57. Li, H. (2018). Minimap2: pairwise alignment for nucleotide sequences. Bioinformatics *34*, 3094–3100.

58. Patro, R., Duggal, G., Love, M.I., Irizarry, R.A., and Kingsford, C. (2017). Salmon provides fast and bias-aware quantification of transcript expression. Nat. Methods *14*, 417–419.

59. Van Rossum, G., and Drake, F.L. (2009). Python 3 Reference Manual (CreateSpace).

60. Schindelin, J., Arganda-Carreras, I., Frise, E., Kaynig, V., Longair, M., Pietzsch, T., Preibisch, S., Rueden, C., Saalfeld, S., Schmid, B., et al. (2012). Fiji: an open-source platform for biological-image analysis. Nat. Methods *9*, 676–682.

61. Virtanen, P., Gommers, R., Oliphant, T.E., Haberland, M., Reddy, T., Cournapeau, D., Burovski, E., Peterson, P., Weckesser, W., Bright, J., et al. (2020). SciPy 1.0: Fundamental Algorithms for Scientific Computing in Python. Nat. Methods *17*, 261–272.

62. Wolf, F.A., Angerer, P., and Theis, F.J. (2018). large-scale single-cell gene expression data analysis. Genome Biol. *19*, 15.

63. Love, M.I., Huber, W., and Anders, S. (2014). Moderated estimation of fold change and dispersion for RNA-seq data with DESeq2. Genome Biol. *15*, 550.

64. R Core Team (2022). R: A Language and Environment for Statistical Computing (R Foundation for Statistical Computing).

65. Huber, W., Carey, V.J., Gentleman, R., Anders, S., Carlson, M., Carvalho, B.S., Bravo, H.C., Davis, S., Gatto, L., Girke, T., et al. (2015). Orchestrating high-throughput genomic analysis with Bioconductor. Nat. Methods *12*, 115–121.

66. NCBI Resource Coordinators (2013). Database resources of the National Center for Biotechnology Information. Nucleic Acids Res. *41*, D8–D20.

67. Durinck, S., Spellman, P.T., Birney, E., and Huber, W. (2009). Mapping identifiers for the integration of genomic datasets with the R/Bioconductor package biomaRt. Nat. Protoc. *4*, 1184–1191.

68. Korotkevich, G., Sukhov, V., Budin, N., Shpak, B., Artyomov, M.N., and Sergushichev, A. (2021). Fast Gene Set Enrichment Analysis. Preprint at bioRxiv. https://doi.org/10.1101/060012.

69. Subramanian, A., Tamayo, P., Mootha, V.K., Mukherjee, S., Ebert, B.L., Gillette, M.A., Paulovich, A., Pomeroy, S.L., Golub, T.R., Lander, E.S., and Mesirov, J.P. (2005). Gene set enrichment analysis: A knowledge-based approach for interpreting genome-wide expression profiles. Proc. Natl. Acad. Sci. USA *102*, 15545–15550.

70. Stirling, D.R., Swain-Bowden, M.J., Lucas, A.M., Carpenter, A.E., Cimini, B.A., and Goodman, A. (2021). CellProfiler 4: improvements in speed, utility and usability. BMC Bioinf. *22*, 433.

71. Kats, I., Vento-Tormo, R., and Stegle, O. (2021). SpatialDE2: Fast and Localized Variance Component Analysis of Spatial Transcriptomics. Preprint at bioRxiv. https://doi.org/10.1101/2021.10.27.466045.

72. Stephens, M. (2017). False discovery rates: a new deal. Biostatistics *18*, 275–294.

73. Dougherty, J.D., Schmidt, E.F., Nakajima, M., and Heintz, N. (2010). Analytical approaches to RNA profiling data for the identification of genes enriched in specific cells. Nucleic Acids Res. *38*, 4218–4230.

74. Nowicka, M., and Robinson, M.D. (2016). DRIMSeq: a Dirichlet-multinomial framework for multivariate count outcomes in genomics. F1000Res. *5*, 1356. https://doi.org/10.12688/f1000research.8900.2.

75. Haenseler, W., Zambon, F., Lee, H., Vowles, J., Rinaldi, F., Duggal, G., Houlden, H., Gwinn, K., Wray, S., Luk, K.C., et al. (2017). Excess α-synuclein compromises phagocytosis in iPSC-derived macrophages. Sci. Rep. *7*, 9003.

76. Fedele, S., Collo, G., Behr, K., Bischofberger, J., Müller, S., Kunath, T., Christensen, K., Gündner, A.L., Graf, M., Jagasia, R., and Taylor, V. (2017). Expansion of human midbrain floor plate progenitors from induced pluripotent stem cells increases dopaminergic neuron differentiation potential. Sci. Rep. *7*, 6036.

77. Williamson, M.G., Madureira, M., McGuinness, W., Heon-Roberts, R., Mock, E.D., Naidoo, K., Cramb, K.M.L., Caiazza, M.C., Malpartida, A.B., Lavelle, M., et al. (2023). Mitochondrial dysfunction and mitophagy defects in *LRRK2-R1441C* Parkinson's disease models. Hum. Mol. Genet. *32*, 2808–2821.

78. atarashansky (2022). SCTransformPy.

79. Traag, V.A., Waltman, L., and van Eck, N.J. (2019). From Louvain to Leiden: guaranteeing well-connected communities. Sci. Rep. *9*, 5233.

80. Dong, K., and Zhang, S. (2022). Deciphering spatial domains from spatially resolved transcriptomics with an adaptive graph attention auto-encoder. Nat. Commun. *13*, 1739.

81. Scrucca, L., Fop, M., Murphy, T.B., and Raftery, A.E. (2016). mclust 5: Clustering, Classification and Density Estimation Using Gaussian Finite Mixture Models. R J. *8*, 289–317.

82. Caglayan, E., Liu, Y., and Konopka, G. (2022). Ambient RNA Analysis Reveals Misinterpreted and Masked Cell Types in Brain Single-Nuclei Datasets. Preprint at bioRxiv. https://doi.org/10.1101/2022.03.09.483658.

83. Szklarczyk, D., Gable, A.L., Lyon, D., Junge, A., Wyder, S., Huerta-Cepas, J., Simonovic, M., Doncheva, N.T., Morris, J.H., Bork, P., et al. (2019). STRING v11: protein–protein association networks with increased coverage, supporting functional discovery in genome-wide experimental datasets. Nucleic Acids Res. *47*, D607–D613.

84. Mancarci, O. (2019). homologene: Quick Access to Homologene and Gene Annotation Updates.

85. Kanehisa, M., and Goto, S. (2000). KEGG: kyoto encyclopedia of genes and genomes. Nucleic Acids Res. *28*, 27–30.

86. Gene Ontology Consortium (2021). The Gene Ontology resource: enriching a GOld mine. Nucleic Acids Res. *49*, D325–D334.

87. Nectow, A.R., Moya, M.V., Ekstrand, M.I., Mousa, A., McGuire, K.L., Sferrazza, C.E., Field, B.C., Rabinowitz, G.S., Sawicka, K., Liang, Y., et al. (2017). Rapid Molecular Profiling of Defined Cell Types Using Viral TRAP. Cell Rep. *19*, 655–667.

STAR★METHODS

KEY RESOURCES TABLE

REAGENT or RESOURCE	SOURCE	IDENTIFIER
Antibodies		
anti-eGFP antibody (clone 19C8)	Heintz Lab; Rockefeller University	RRID:AB_2716737
anti-eGFP antibody (clone 19F7)	Heintz Lab; Rockefeller University	RRID:AB_2716736
anti-TH	Abcam	RRID:AB_1524535
anti-GFP	Invitrogen	RRID:AB_221569
anti-CASR	Abcam	RRID:AB_2071489
DAPI	Thermo Fisher Scientific	RRID:AB_2307445
anti-TYROBP/DAP12	Abcam	RRID:AB_3086739
anti-MAP2	Abcam	RRID:AB_2138147
anti-TH	Millipore	RRID:AB_90755
Alexa Fluor-conjugated anti-rabbit/chicken secondary antibodies	Thermo Fisher Scientific	RRID:AB_2536183, RRID:AB_2921074
Chemicals, peptides, and recombinant proteins		
R 568	Tocris	Cat# 3815; CAS 177172-49-5
Deposited data		
Raw and analyzed sequencing data	This Paper	GEO: GSE215276 and CNGBdb: CNP0003397
CASR ICC data	This Paper	https://doi.org/10.5281/zenodo.10476097
CASR IHC data	This Paper	https://doi.org/10.5281/zenodo.10401754
TYROBP IHC data	This Paper	https://doi.org/10.5281/zenodo.10401777
Fura-2-AM data	This Paper	https://doi.org/10.5281/zenodo.10669197
Astrocyte TRAP data	Sakers et al.[24]	GSE74456
GABAergic neuron RiboTag data	Paul et al.[38]	N/A
Oligodendrocyte RiboTag data	Voskuhl et al.[39]	GSE118451
Microglia TRAP data	Vasek et al.[56]	GSE161460
GABAergic neuron TRAP data	Ouwenga et al.[40]	GSE121162
Experimental models: Organisms/strains		
Rosa26fsTRAP mice (B6.129S4-Gt(ROSA)26Sortm1(CAG-EGFP/Rpl10a,-birA)Wtp/J)	JAX	*RRID:IMSR_JAX:022367*
DATIREScre mice (B6.SJL-Slc6a3tm1.1(cre)Bkmn/J)	JAX	*RRID:IMSR_JAX:006660*
SNCA-OVX mice (B6.Cg-Tg(SNCA)OVX37Rwm Sncatm1Rosl/J)	JAX	*RRID:IMSR_JAX:023837*
Experimental models: Cell lines		
JR053 (Control iPSC line 1)	EBiSC	JR053-1
SFC067-03 (Control iPSC line 2)	EBiSC	SFC067-03-01
SFC156-03 (Control iPSC line 3)	EBiSC	SFC156-03-01
SFC856-03 (Control iPSC line 4)	EBiSC	SFC856-03-01
SFC831-03 (SNCA triplication iPSC line - clone 1)	EBiSC	SFC831-03-01
SFC831-03 (SNCA triplication iPSC line - clone 3)	EBiSC	SFC831-03-03
SFC831-03 (SNCA triplication iPSC line - clone 5)	EBiSC	SFC831-03-05
Oligonucleotides		
See Table S4		
Software and algorithms		
Analysis code	This Paper	https://doi.org/10.5281/zenodo.10401701
Minimap2 v2.18	Li[57]	RRID:SCR_018550

(*Continued on next page*)

Continued

REAGENT or RESOURCE	SOURCE	IDENTIFIER
Salmon v1.4.0	Patro et al.[58]	RRID:SCR_017036
Python v3.9	Van Rossum et al.[59]	RRID:SCR_008394
Fiji v1.53q	Schindelin et al.[60]	RRID:SCR_002285
SciPy v1.9.0	Virtanen et al.[61]	RRID:SCR_008058
Scanpy v1.9.1	Wolf et al.[62]	RRID:SCR_018139
DESeq2 v1.36.0	Love et al.[63]	RRID:SCR_015687
R v4.2.1	R Core Team[64]	RRID:SCR_001905
Bioconductor v3.15	Huber et al.[65]	RRID:SCR_006442
Homologene v1.4.68.19.3.27	NCBI Resource Coordinators[66]	RRID:SCR_002924
biomaRt v2.52.0	Durinck et al.[67]	RRID:SCR_019214
Fgsea v1.22.0	Korotkevich et al.[68]	RRID:SCR_020938
MSigDB v7.5.1	Subramanian et al.[69]	RRID:SCR_016863
Guppy v4.5.2	Oxford Nanopore Technologies Ltd	https://community.nanoporetech.com/docs/prepare/library_prep_protocols/Guppy-protocol/v/gpb_2003_v1_revax_14dec2018/guppy-software-overview
CellProfiler v4.2.5	Stirling et al.[70]	RRID:SCR_007358
SpatialDE2	Kats et al.[71]	https://github.com/PMBio/SpatialDE
Ashr v2.2-63	Stephens, M[72]	https://cran.r-project.org/web/packages/ashr/index.html
pSI v1.1	Dougherty et al.[73]	https://www.rdocumentation.org/packages/pSI/versions/1.1
DRIMSeq v1.30.0	Nowicka and Robinson et al.[74]	https://bioconductor.org/packages/release/bioc/html/DRIMSeq.html
Other		
Resource website	This Paper	https://spatialbrain.org/

RESOURCE AVAILABILITY

Lead contact

Further information and requests for resources and reagents should be directed to and will be fulfilled by the lead contact, Richard Wade-Martins (richard.wade-martins@dpag.ox.ac.uk).

Materials availability

This paper generated a cross between B6.129S4-Gt(ROSA)26Sortm1(CAG-EGFP/Rpl10a,-birA)Wtp/J (RRID:IMSR_JAX:022367), B6.SJL-Slc6a3tm1.1(cre)Bkmn/J (RRID:IMSR_JAX:006660) and B6.Cg-Tg(SNCA)OVX37Rwm Sncatm1Rosl/J (RRID:IMSR_JAX:023837). All three lines are available from JAX.

iPSC lines used as part of this study are available from the authors. Please contact the lead contact for access/more details.

Data and code availability

- All raw data from TRAP experiments have been uploaded to the Gene Expression Omnibus (GEO accession number: GSE215276). The Stereo-seq raw data that supports the findings of this study have been deposited into CNGB Sequence Archive (CNSA) of China National GeneBank DataBase (CNGBdb) with accession number CNP0003397. All processed data, including results of all analyses are provided at spatialbrain.org. Imaging data of CASR and TYROBP immunohistochemistry samples have been deposited for public access at Zenodo (CASR IHC: https://doi.org/10.5281/zenodo.10401754, CASR ICC: https://doi.org/10.5281/zenodo.10476098, TYROBP IHC: https://doi.org/10.5281/zenodo.10401777).
- All original code has been deposited at https://github.com/legbar/spatialbrain and is publicly available as of the date of publication (https://doi.org/10.5281/zenodo.10401701). Protocols for laboratory collection and processing of samples as described in this study are published as a collection at protocols.io (https://doi.org/10.17504/protocols.io.36wgqj75kvk5/v1).
- Any additional information required to reanalyze the data reported in this work paper is available from the lead contact upon request.

EXPERIMENTAL MODEL AND STUDY PARTICIPANT DETAILS

Animals

All experiments and procedures conducted on animals were carried out in accordance with United Kingdom Home Office regulations under the Animal (Scientific Procedures) Act (1986), and were approved by the local ethical review board of the Department of Physiology, Anatomy and Genetics at the University of Oxford. All mice were housed in the University of Oxford Biomedical Services Building. Mice had access to standard food and water *ad libitum*. Mouse holding rooms were maintained at 22°C and 60 to 70% humidity on a 12-h light-dark cycle. All mice were bred on a C57/BL6 background (MGI Cat# 2159769, RRID:MGI:2159769). For all experiments, animals of both sexes were used unless indicated otherwise. Animals used for both Stereo-seq and TRAP technologies were littermates.

iPSC-derived dopamine neurons

The generation and characterization of iPSCs from healthy individuals or PD patients carrying a triplication of the SNCA locus were described in Haenseler et al.[75] The three control and three SNCA-Triplication patient lines underwent a differentiation process following the protocol described by Fedele et al.[76] with slight modifications as outlined in Williamson et al.[77] Briefly, the cells were initially patterned for 10 days, followed by expansion of midbrain floor plate progenitors for 19 days. Subsequently, the progenitors were differentiated for an additional 10 days, then replated and matured for a further 5 weeks until reaching DIV 60 for imaging.

METHOD DETAILS

Transgenic model generation

Homozygous Rosa26^{fsTRAP} mice were bred with homozygous DAT^{IREScre} mice to generate heterozygous Rosa26^{fsTRAP}::DAT^{IREScre} offspring that were used for TRAP experiments. Rosa26^{fsTRAP} parents were crossed and bred to be hemizygous *hSNCA*+ (*SNCA*-OVX): Offspring were a mixture of hemizygous *hSNCA*+ and *hSNCA*-. All animals were wild-type mouse *Snca*$^{+/+}$, due to the position of the ROSA26-eGFP-L10a locus being on the same chromosome as *Snca* (chromosome 6). Routine ear-clipping, digestion and PCR-genotyping was performed as described in Hunn et al.[7] Primer sequences used for confirmation of transgene expression are supplied in Table S4.[8,9,34,35]

TRAP

Mice were sacrificed by cervical dislocation, the ventral midbrain and striatal tissue were rapidly dissected and affinity purification of eGFP-tagged polysomes was performed.[20] Briefly, dissected tissue was immediately dounce homogenized in lysis buffer containing 20 mM HEPES KOH, 150 mM KCl, 10 mM MgCl2, 0.5 mM DTT, 100 μg/mL cycloheximide, RNasin (Promega) and SUPERase-in (Life Technologies) and Complete-EDTA-free protease inhibitors (Roche) in Rnase-free water. The lysate was cleared by two-stage centrifugation for 10 min at 2,000 x *g* and 20,000 x *g*. Each lysate was incubated with monoclonal anti-GFP antibodies (Heintz Lab; Rockefeller University Cat# Htz-GFP-19C8 and Htz-GFP-19F7, RRID:AB_2716737 and RRID:AB_2716736), coated on paramagnetic beads through a streptavidin-biotin-protein L linker (Pierce; Thermo Fisher Scientific) for 18 h at 4°C. To remove non-specifically bound material, including RNA, beads were washed 6 times in a high-salt solution containing 20 mM HEPES KOH (pH 7.4), 350 mM KCl, 10 mM MgCl2, 1% NP-40, 0.5 mM DTT, 100 g/mL cycloheximide, and Rnasin and Superasin. RNA was extracted using the Rneasy Micro Plus kit (Qiagen). RNA quantity and integrity were measured using the Quant-it RiboGreen RNA Assay Kit (Thermo Fisher) and Agilent 2100 Bioanalyzer, respectively. RNA-seq library preparation was performed using the NEBNext Ultra II Directional RNA kit. Transcript level quantification was performed using Salmon (v1.4.0, RRID:SCR_017036).[58]

Long-read sequencing and data processing

Twelve TRAP samples and three TOTAL samples were sequenced using the Oxford Nanopore Technologies MinION platform. TRAP samples were equally divided by age and genotype (N = 3 per age:genotype). Library preparation was performed using the cDNA-PCR kit (SQK-PCS109). Raw fast5 data was basecalled and demultiplexed using Guppy (v4.5.2). Read data from FASTQ files were aligned to the mm10 genome (Gencode M25 GRCm38.p6) using minimap2 (v2.18, RRID:SCR_018550).[57] Transcript level quantification was then performed using Salmon (v1.4.0, RRID:SCR_017036).[58]

Stereo-seq library preparation and sequencing

Stereo-seq libraries were prepared using one chip per brain, across 18 brains in total.[18] In brief, Stereo-seq samples were first prepared by collecting postmortem mouse brains and flash-freezing at −80°C. 10 μm tissue sections were collected −3.5 mm from bregma (to optimize capture of DA neurons in the SN and VTA) using a Leica CM1950 cryostat and adhered to each Stereo-seq chip (BGI Research). The chip was placed on a warming plate at 37°C for 3 min and fixed in methanol at −20°C for 30 min. The chip was incubated with 100 μL 0.1% pepsin at 37°C for 12 min for permeabilization and washed with 0.1× SSC buffer containing 0.05 U/μL RNase inhibitor. RNA captured by the DNA nanoball on the chip was reverse transcribed at 42°C for 90 min. Tissue was removed from the chip by incubating with tissue removal buffer at 55°C for 10 min. After washing with 0.1× SSC buffer, the chip with cDNA was incubated with 400 μL cDNA release buffer at 55°C for 4 h cDNA was purified and amplified using cDNA primer. A total of

20 ng of cDNA was fragmented, amplified, and purified to generate each cDNA sequencing library. The cDNA library was sequenced on an MGI DNBSEQ-Tx sequencer with the read length of 50 bp for read 1 and 100 bp for read 2.

Immunohistochemistry

Mice were anesthetized by intraperitoneal injection of 150 μL pentobarbital. Upon loss of the pedal withdrawal reflex, the thoracic cavity was opened, and 25 mL of phosphate-buffered saline (PBS) was administered transcardially, followed by 25 mL of 4% paraformaldehyde (PFA), diluted in PBS. The brain was extracted and stored overnight in 4% PFA at 4°C. Brain tissue was next dehydrated, and paraffin embedded through graded alcohols, histoclear (ThermoFisher Scientific) and paraffin solution. Tissue blocks were finally sectioned at 7 μm using a Leica microtome (Leica Microsystems, Wetzlar, Germany) and mounted on glass slides (VWR, Superfrost Plus).

Sections were prepared for immunofluorescence by performing dewaxing in histoclear, rehydration in graded alcohols, antigen retrieval by microwave heat (20 min) and citrate buffer (ab96678, Abcam). Tissue was blocked for 1 h at room temperature using 10% donkey serum in TBS. Primary antibodies to TH (Abcam Cat# ab76442, RRID:AB_1524535, 1:500), GFP (Thermo Fisher Scientific Cat# A-11122, RRID:AB_221569, Invitrogen, 1:1000), CASR (Abcam Cat# ab79038, RRID:AB_2071489, 1:100) and TYROBP/DAP12 (Abcam Cat# ab283679, RRID:AB_3086739, 1:100) were prepared in blocking solution and incubated overnight at 4°C. Slides were washed using TBS and incubated in secondary antibodies (Alexa Fluor-conjugated anti-rabbit/chicken A-31573, RRID:AB_2536183 and A78952, RRID:AB_2921074 1:1000) and DAPI (Thermo Fisher Scientific Cat# D3571, RRID:AB_2307445, 1:5000) for 1 h at room temperature. Slides were washed and coverslips mounted using FluorSave mounting medium (Millipore, Massachusetts, United States of America).

For detection and quantification of Tyrobp/Dap12-positive cells and analysis of Casr-positivity, two custom pipelines were built using CellProfiler (RRID:SCR_007358), provided in the accompanying GitHub repository to this manuscript.[70] To calculate the Casr cytoplasm:nucleus ratio, a 10 pixel-wide cytoplasmic object was created, originating from each DAPI-positive spot (nucleus). Each nucleus and cytoplasm was classified either as TH-positive or TH-negative, based on overlapping cytoplasmic TH signal. Objects with only partial TH overlap were filtered, to ensure accurate classification. The maximal Casr intensity for each object was recorded and summarized for each mouse by calculating the mean across objects. The Casr cytoplasm:nucleus ratio represents the ratio of these means.

Immunocytochemistry

After R568 treatment, the iPSC derived DA neurons were fixed in 4% PFA. Cells were permeabilized for 10 min a solution of 5% NDS, 1% BSA and 0.5% Triton X-100. Samples were blocked in a solution of 5% NDS and 1% BSA for 1 h. Cells were then incubated for 16 h O/N at 4°C with the following primary antibodies: CASR (Abcam Cat# ab79038, RRID:AB_2071489, 1:500), MAP2 (Abcam Cat# ab92434, RRID:AB_2138147, 1:1000), tyrosine hydroxylase (Millipore Cat# AB1542, RRID:AB_90755, 1:500). Cells were washed twice in PBS and then incubated in secondary antibodies and DAPI for 1.5 h at RT. Cells were washed 3 times and stored in fresh PBS until imaging. Cells were imaged using the OperaPhenix (PerkinElmer).

Fura-2

Fura-2 a.m. was prepared to 5 mM concentration in calcium-free HBSS supplemented with 20 mM HEPES. It was then diluted to the final concentration of 2.5 mM in Neurobasal medium supplemented with B27 and L-glutamine, with DMSO (0.1%) or the CaSR positive modulator R568 (10 μM).

iPSC-derived DA neurons were incubated in the solution of Fura-2 a.m. and drug for 1 h at 37°C, 5% CO_2 and then imaged on a FlexStation 3 Multi-Mode Microplate Reader (Molecular Devices) at 37°C. The dye was excited at 340 nm and 380 nm and was detected at 510 nm. Each well was imaged every 4 s for 100 s and injected with ionomycin (final concentration 5 μM) after a baseline of 28 s.

For the analysis, the 340/380 ratio was computed, and then the baseline was subtracted from all the timepoints, to obtain a normalized trace for each well. The maximum intensity (peak amplitude) of the normalized trace was found and the area under the curve (AUC) was calculated using the left rectangular approximation method.

Stereo-seq data processing

Raw gene-by-spot data per sample were aggregated to create a 2-dimensional image of RNA signal for each sample using custom Python (v3.9.0, RRID:SCR_008394) scripts. To segment individual cells, each image was subjected to a processing pipeline written in Python (workflow illustrated in Figure S1). Steps taken: *Mask generation from unspliced counts:* Gaussian filter (sigma = 5), background subtraction (white tophat, 50 pixels), Otsu thresholding, conversion to mask, fill holes, watershed. *Mask generation from spliced + unspliced counts:* As for unspliced counts. Watershed boundaries from the spliced + unspliced mask were then subtracted from the unspliced mask. Objects were retained from the spliced + unspliced mask that overlapped with the unspliced mask. Each cell was labelled using the label function in SciPy (v1.9.0, RRID:SCR_008058). Raw gene-by-spot data were then aggregated to the gene-by-cell level and imported into scanpy (v1.9.1, RRID:SCR_018139).[62]

The initial Stereo-seq dataset contained 497,766 cells. In a first round of filtering, low complexity and putative doublet/triplet cells were filtered. To remove low complexity cells, a minimum gene detection cutoff of 200 was selected. To remove putative doublet/triplet cells, a maximum gene detection cutoff was set on a per-brain basis to the median number of genes detected +4 median absolute deviations. After first round filtering, 415,402 cells remained. Count data were subsequently processed using SCVI,

including sample brain of origin as a categorical covariate, and the number of genes detected per cell as a continuous covariate.[78] A uniform manifold projection (UMAP) was generated for cells from each mouse brain and overlaid, showing a similar pattern of separation (Figure S1A).

Cell type identification was performed in two rounds. In a first pass, leiden clustering was performed at iteratively greater resolutions.[79] Cell types without clear spatial organization e.g., some glial types, were annotated based on marker gene enrichment. Remaining cells were then processed using SEDR in order to include spatial information in the clustering process.[80] Mclust was used for clustering spatially defined cell types.[81] If a cluster contained fewer than 200 cells, it was considered final and no further subclustering was performed. Dopaminergic neurons were labelled according to their anatomical region (SN and VTA), based on their spatial coordinates.

For differential expression analysis in Stereo-seq samples, gene counts were normalized to the total number of counts per cell and log-transformed. Marker genes for each cluster were identified using the Wilcoxon rank-sum test, providing two-sided p values. The identity of each cell type was annotated by integrating marker gene data with previous literature and by confirming the spatial distribution of clustered cells.

A second round of cell filtering was performed after clustering to remove cells that were enriched in both *Snap25* and *Plp1*. We suspected that these cells represent neuronal/glial contaminated mixtures, as previously reported in single cell data.[82] After second-round filtering, 355,307 cells remained.

Spatially variable gene detection

Spatially variable genes were identified using SpatialDE2 with default settings. Coordinates and full expression matrices of each brain were supplied, divided by cell type. To combine results from separate samples, a meta-analysis was performed on the raw p values from each sample, using Fisher's method. The Benjamini & Hochberg correction for multiple comparisons was subsequently used and genes were considered spatially variable with an adjusted p value of <0.01.

Stereo-seq cell type abundance analysis

To test for differential abundance of cell types between age groups, we used mixed effects modeling of associations of single cells (MASC). MASC tests whether cell type membership of individual cells is influenced by an experimental covariate of interest, while accounting for technical covariates and biological variation. We specified mouse genotype as a fixed covariate and mouse of origin as a random effect in the generalized, mixed-effect model. Changes in cell type abundance were considered significant at FDR-$P < 0.01$.

Differential gene expression analysis

Differential gene expression analysis in TRAP samples (including calculation of gene enrichment and depletion, relative to tissue homogenate RNA) was performed using DESeq2 (v1.36.0, RRID:SCR_015687) in R (v4.2.1, RRID:SCR_001905) with Bioconductor (v3.15, RRID:SCR_006442). Adaptive shrinkage of log fold change estimates was performed using ashr. The following settings were changed from defaults: minReplicatesForReplace = Inf, cooksCutoff = Inf, filterFun = ihw, lfcThreshold = $\log_2(1.05)$. Genes were classed as significantly differentially expressed with an FDR-adjust p value <0.01. Protein-protein interactions were obtained using STRINGdb (version 11) with a minimum confidence threshold of 0.4.[83]

Specificity index (pSI) calculation

To calculate the specificity index of genes detected within TRAP/RiboTag datasets of dopaminergic neurons and other cell types within midbrain, pSI (v1.1) was used with default settings.[22,24,38–40,73] Genes were considered significantly specifically expressed with an FDR-adjusted p value <0.01.

Differential transcript usage analysis

Differential transcript usage was performed using DRIMSeq (v1.24.0). To consider only genes containing more than 1 isoform, with a minimum level of expression, the following parameters were used: min_samps_gene_expr = n * 0.75, min_gene_expr = 10, min_samps_feature_expr = 10, min_feature_expr = 10, min_samps_feature_prop = 10, min_feature_prop = 0.1.

GWAS prioritization analysis

A list of 303 genes (sourced from Nalls et al., 2019 supplementary materials), containing SNPs at an $r^2 > 0.5$ and located within ±1 Mb of 107 common risk variants for sporadic PD was used for prioritization analysis.[42] To convert between human and mouse gene symbols, homologene (v1.4.68.19.3.27, RRID:SCR_002924) and biomaRt (v2.52.0, RRID:SCR_019214) were used.[67,84] TRAP enrichment (measured as the product of the $\log_2$ fold-change and FDR-adjusted p value) and specificity indices for DAT-TRAP samples were used for gene prioritization, per lead SNP.

Gene set enrichment analysis

Gene set enrichment analysis was performed using fgsea (v1.22.0, RRID:SCR_020938) with the following parameters: eps = 0, minSize = 10, maxSize = 500, nPermSimple = 10000. Pathway data were obtained from the Molecular Signatures Database (v7.5.1, RRID:SCR_016863), using C2 Canonical Pathways from Kegg and C5 Gene Ontology sets.[85,86]

QUANTIFICATION AND STATISTICAL ANALYSIS

No statistical methods were used to predetermine sample sizes, but our sample sizes for TRAP analyses surpass those reported in previous publications[23,28,87] and our sample sizes for Stereo-seq samples are comparable with or exceed those of similar spatial transcriptomic datasets.[11] All statistical analyses were performed with R (v4.2.1) and Python (v3.9). All p values were modified to an FDR of 1, 5 or 10% as described in the text with the Benjamini & Hochberg method.